# Supplemental Material

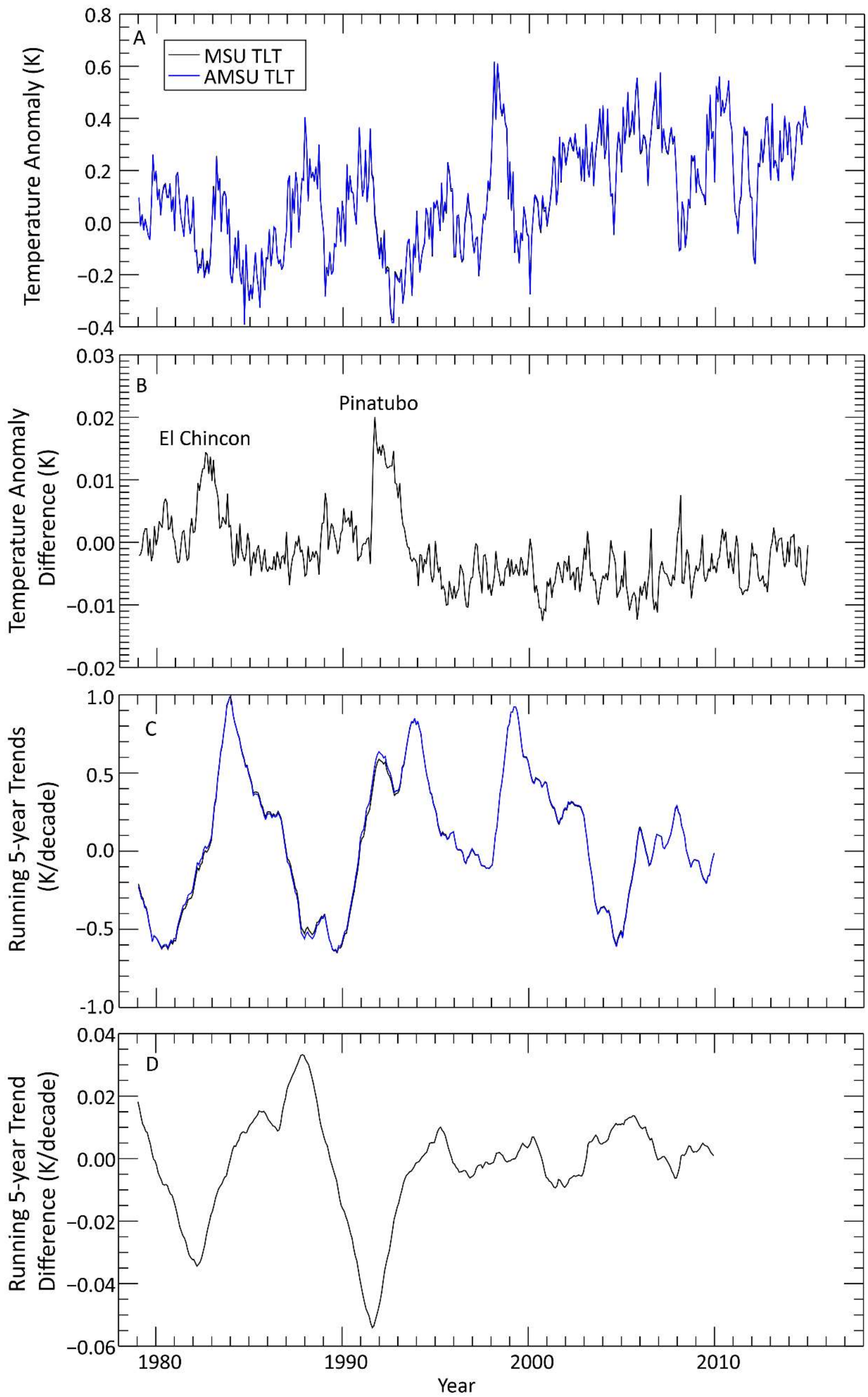
A
MSU TLT
AMSU TLT
Temperature Anomaly (K)
B
El Chincon
Pinatubo
Temperature Anomaly Difference (K)
C
Running 5-year Trends (K/decade)
D
Running 5-year Trend Difference (K/decade)
Year

1

Fig. S1. Comparison of global TLT time series calculated using the MSU and AMSU TLT field of view combination and measurement frequencies. Both time series we calculated using monthly mean output from the ERA-Interim reanalysis as input to our radiative transfer model. Panel A shows the two time series, which are visually indistinguishable. Panel B shows the difference time series (MSU minus AMSU). The two time series are within 0.015K except during the eruptions of El Chincon and and Pinatubo in 1982 and 1991, when substantial stratospheric warming occurred. Panel C shows running 5-year trends of the two time series, with the trend value plotted at the start year for each 5 year period. 5 years is the length of the MSU/AMSU overlap period (1999-2005) that shows anomalous trend difference between the two instrument types. Panel D shows the difference between the 5 year-running trends. Panels C and D show that the observed MSU/AMSU trend difference is not due to different atmospheric weighting, since even the largest trend difference (~0.05K/decade) is much less that the observed MSU/AMSU global trend difference (0.14 K/decade).

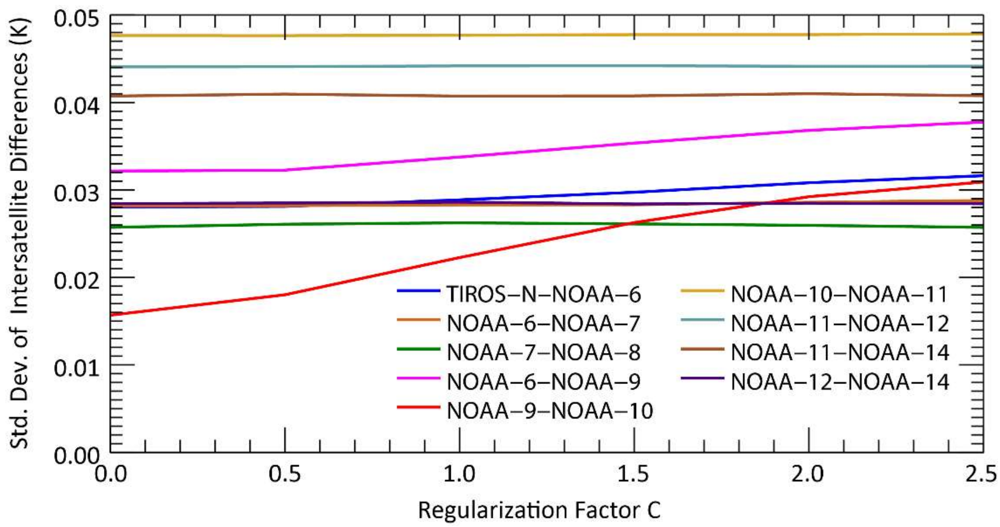


Figure S2. Standard deviation of the instersatellite differences between pairs of MSU satellites as a function of the regularization factor C. The standard deviation is approximately constant for most satellite pairs except for those involving NOAA-09. The NOAA-9 – NOAA-10 values begin at a value much less than from the other pairs, suggesting that some over fitting may be occurring when regularization is not used. When C reaches 1.5, the standard deviation for this pair has increased to a value comparable to the other pairs. This is part of the reason that we choose to use 1.5 as the value for C.

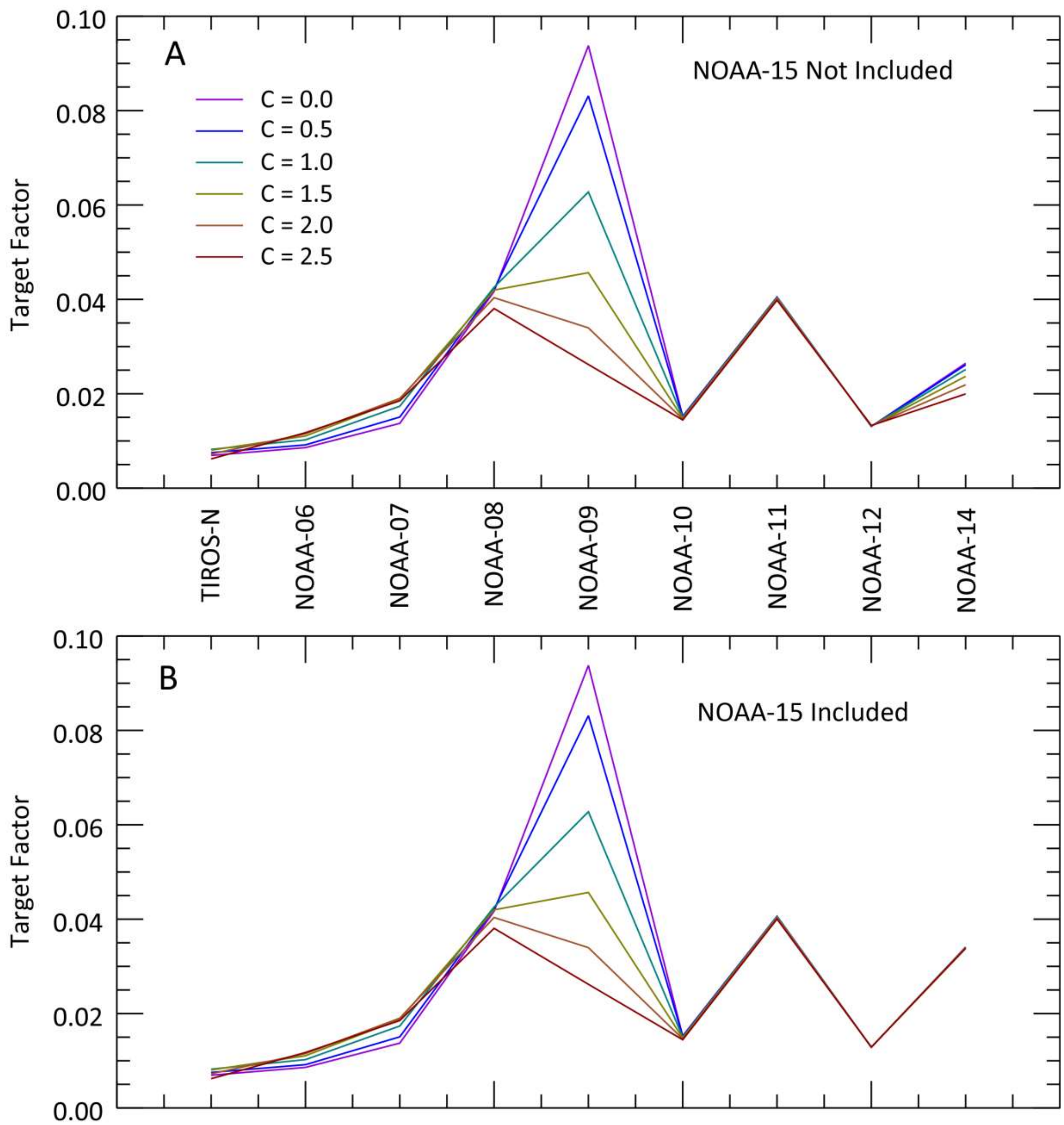


Figure S3. (A) MSU target factors obtained using different values of C. C determines the degree to which the target factors are "pulled" toward zero (see Equation 3, main text). The target factor for NOAA-09 is poorly constrained, and decreases strongly to increasing values of C. Note that the target factors for NOAA-06 and NOAA-07 increase with increasing C, despite being individually pulled toward zero. This is due to their interaction with NOAA-09. When NOAA-15 measurements are not used to help determine the target factor for NOAA-14, it is also relatively sensitive to C, leading to large changes in the final results after 1999. When NOAA-15 data is included (B), the NOAA-14 target factor is well constrained at a larger value, and no longer responds to changes in C.

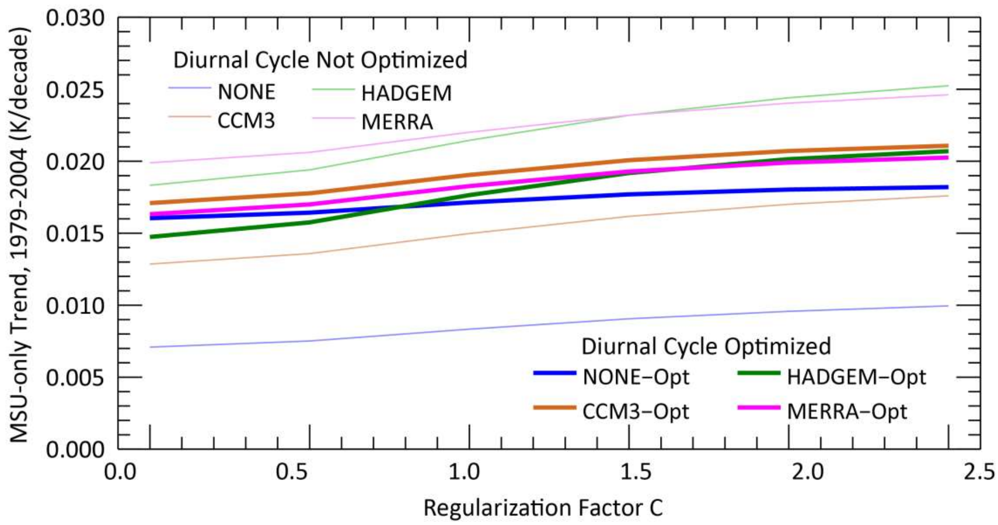


Figure S4. Near Global (60S-60N) MSU-only TLT trend (1979-2004) as a function of regularization factor C. The bold lines are for the DIUR-OPT results, and the light lines show results when the diurnal cycle is not optimized. In all cases, larger values of C lead to larger values of the overall trends. Since we do not know the best value of C exactly, this contributes to the trend uncertainty in the final results. The figure also shows how the diurnal optimization procedure brings results when different diurnal climatologies are used into much better agreement.

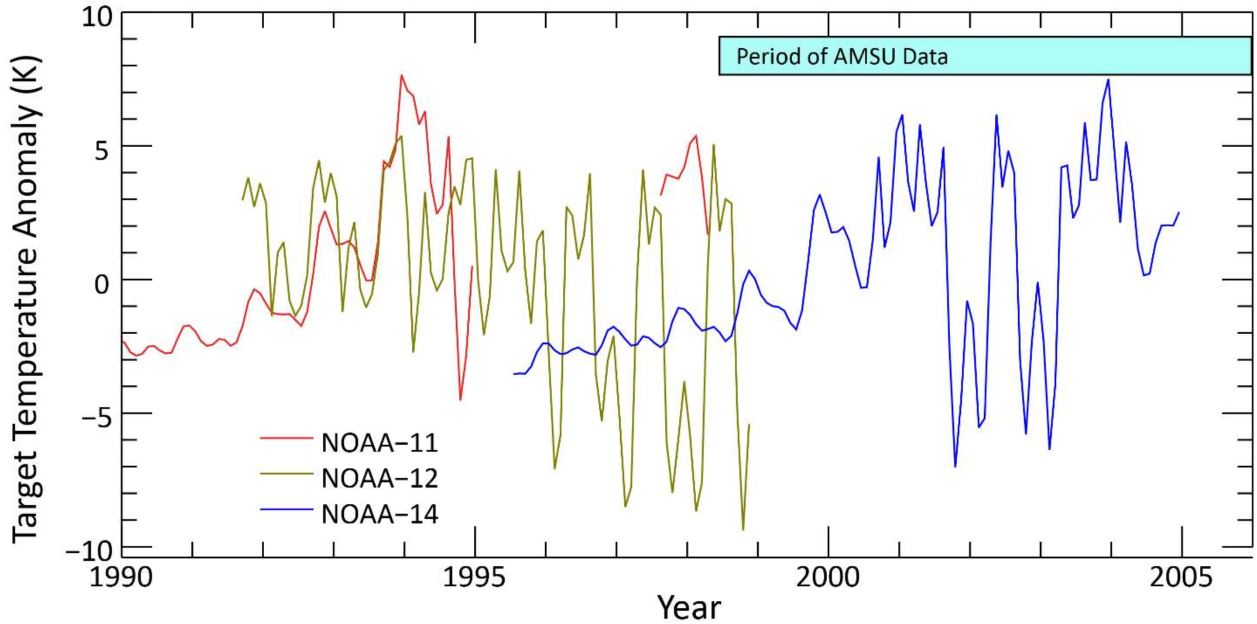


Figure S5. Calibration Target Temperatures for NOAA-11, NOAA-12, and NOAA-14. The fluctuations in target temperature for NOAA-14 are not large until after the end of the NOAA-12 mission. This causes the target factor for NOAA-14 to contains errors large enough to be important when the regression only included MSU data. If we include information from differences between NOAA-14 and merged AMSU data (denoted by the light blue bar), then the period of NOAA-14 data with large target temperature fluctuations is sampled, leading to a better estimate of the target factor.

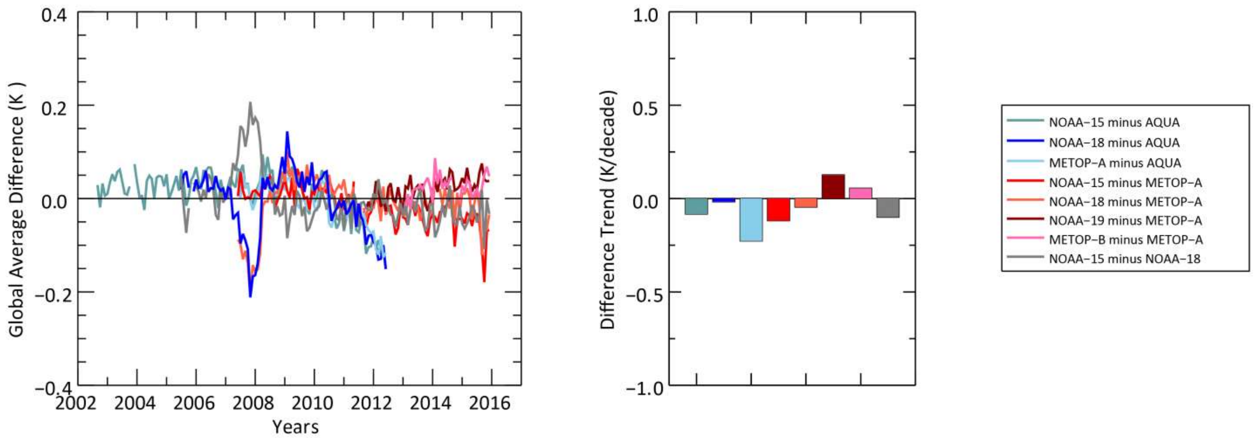


Figure S6. Monthly, near-global (60S-60N) oceanic intersatellite differences. These plots are analogous to Fig. 3, except made with monthly data. With monthly data, it is easy to conclude that NOAA-18 underwent anomalous changes in calibration during 2007 and early 2008.

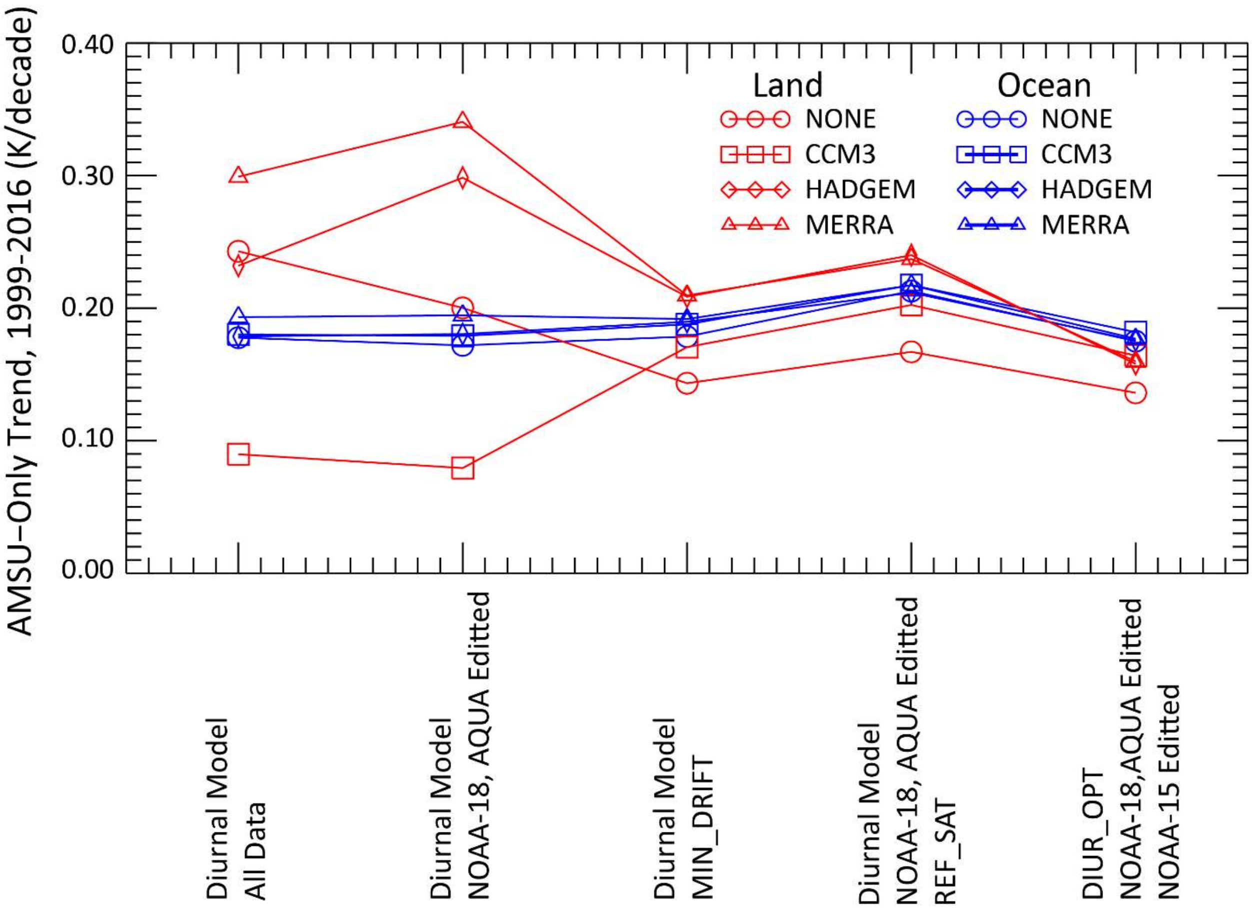


Fig S7. Near-Global (60S – 60N) AMSU Only Trends for different starting diurnal models and merging procedures. The MIN_DRIFT, REF_SAT and DIUR_OPT methods all bring the land trends closer together but have little effect on the ocean trends.

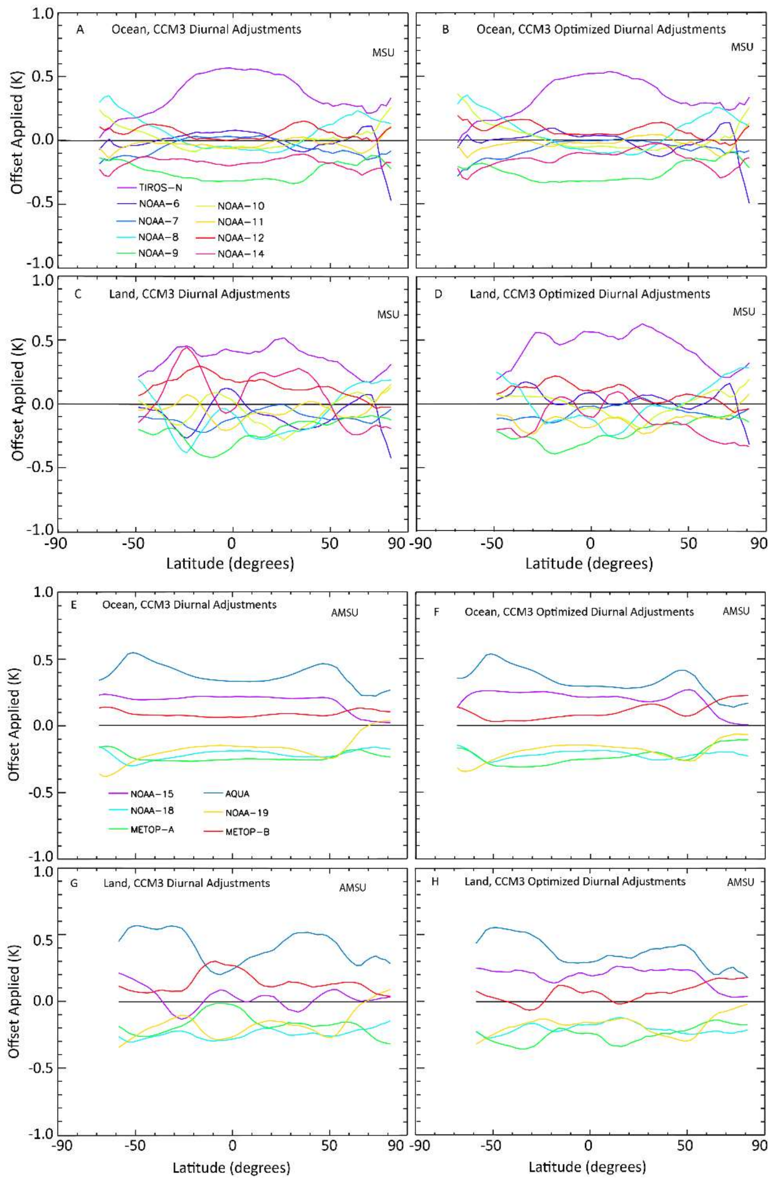


Fig S8. Plots of the offset adjustments applied for each instruments as a function of latitude. Different sets of offset adjustments are calculated for land and ocean scenes. When the optimized diurnal adjustments are used, the differences between land (left column) and ocean (right column) offsets are reduced, and the land offsets vary less with latitude.

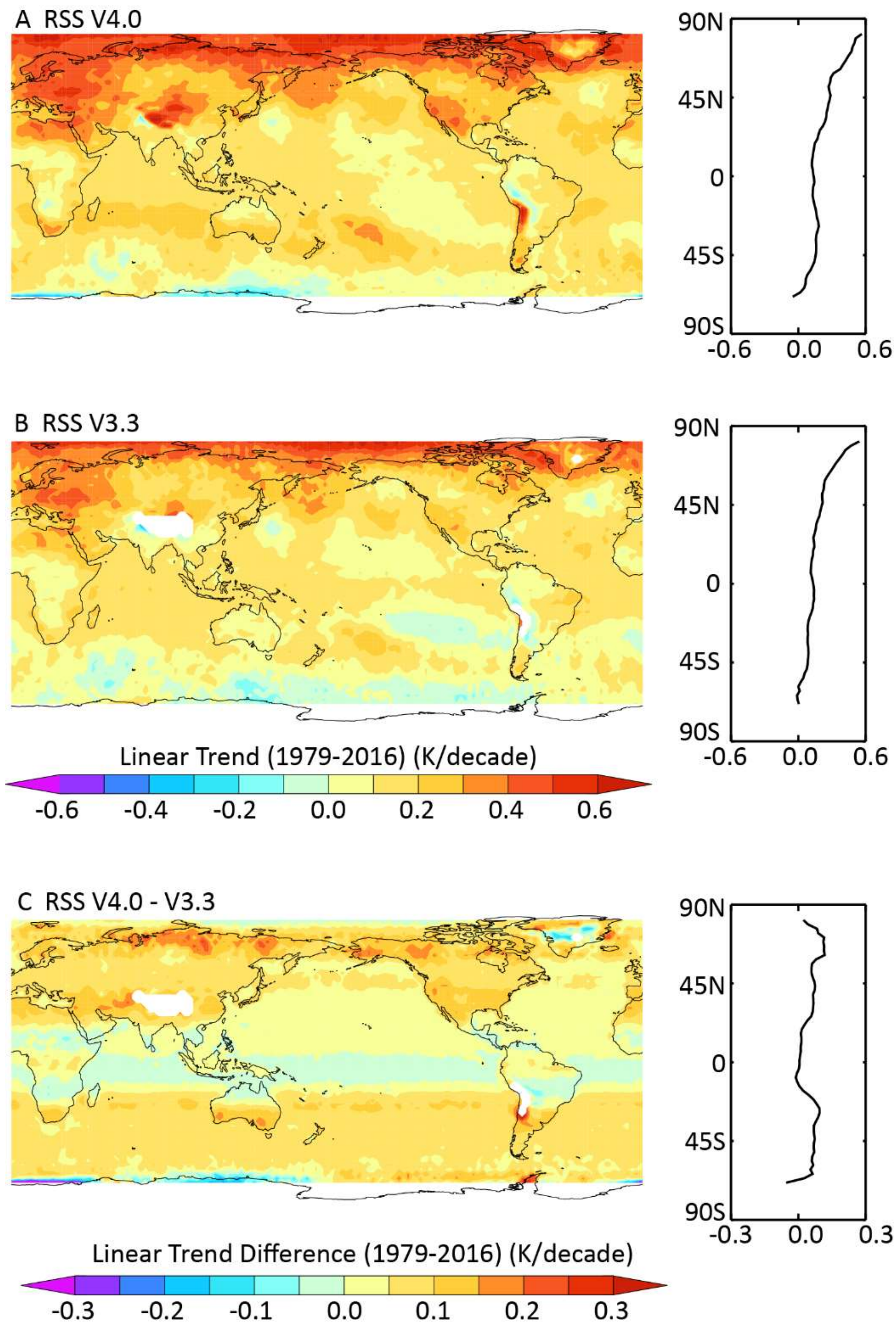


Figure S9. Comparsion of linear trend (1979-2016) maps for the old and new RSS versions of TLT. Panel A shows the trend map for RSS V4.0, B shows the map for RSS V3.3, and panel shows the maps of the trend differences. Most of the increased warming in V4.0 occurs outside of the deep tropics.

**Table S1.** AMSU-only global (70S to 80N) Trends (1999-2016) for different cutoff times for the MIN_DRIFT approach.

| Last NOAA-15 Month | Trend (K/decade) |
|---|---|
| June 2003 | 0.185 |
| December 2003 | 0.183 |
| June 2004 | 0.185 |
| December 2004 | 0.183 |

**Table S2.** Scaling ratio between total column water vapor and TLT on intermediate (3 month to 3 year) time scales, and for 1988-2016 trends. Units are %/K.

| | RSS V4.0 | RSS V3.3 | UAH V6.0 | UAH V5.6 |
|---|---|---|---|---|
| Interannual Std. Dev. Ratio | 6.48 | 6.45 | 5.99 | 6.39 |
| Trend Ratio (1988-2013) | 8.25+/-1.45 | 10.06+/-1.68 | 12.91+/- 2.15 | 11.18+/-1.86 |